# A first-principles study on defect association and oxygen ion migration of Sm3+ and Gd3+ co-doped ceria

**ARTICLE** *in* JOURNAL OF PHYSICS CONDENSED MATTER · MAY 2013

Impact Factor: 2.35 · DOI: 10.1088/0953-8984/25/22/225401 · Source: PubMed



**8 AUTHORS**, INCLUDING:

Mamoru Sakaue
Osaka University
**44** PUBLICATIONS **230** CITATIONS
SEE PROFILE

Susan Aspera
Osaka University
**25** PUBLICATIONS **62** CITATIONS
SEE PROFILE

Triati Wungu
Bandung Institute of Technology
**23** PUBLICATIONS **27** CITATIONS
SEE PROFILE

Hideaki Kasai
Osaka University
**426** PUBLICATIONS **3,183** CITATIONS
SEE PROFILE

A first-principles study on defect association and oxygen ion migration of $Sm^{3+}$ and $Gd^{3+}$ co-doped ceria



2013 J. Phys.: Condens. Matter 25 225401

(http://iopscience.iop.org/0953-8984/25/22/225401)

J. Phys.: Condens. Matter **25** (2013) 225401 (8pp) doi:10.1088/0953-8984/25/22/225401

# A first-principles study on defect association and oxygen ion migration of $Sm^{3+}$ and $Gd^{3+}$ co-doped ceria

**Musa Alaydrus[1], Mamoru Sakaue[1], Susan M Aspera[1], Triati D K Wungu[1], Tran P T Linh[1], Hideaki Kasai[1], Tatsumi Ishihara[2] and Takahiro Mohri[3]**

[1] Department of Precision Science and Technology and Applied Physics, Graduate School of Engineering, Osaka University, Suita, Osaka 565-0871, Japan
[2] International Institute for Carbon-Neutral Energy Research (WPI- I$^2$CNER), Kyushu University, Motooka 744, Nishi-Ku, Fukuoka 819-0395, Japan
[3] Product Technology Development Center, Konica Minolta Technology Center, INC., 1-2 Sakura-Machi, Takatsuki-Shi, Osaka 569-8503, Japan

E-mail: kasai@dyn.ap.eng.osaka-u.ac.jp

Received 23 January 2013, in final form 9 April 2013
Published 9 May 2013
Online at stacks.iop.org/JPhysCM/25/225401

**Abstract**
First-principles calculations based on density functional theory were performed to investigate the co-doping effects of Sm and Gd in ceria on its oxygen ion conduction. The focus of this study is on the interactions between the cation dopants and an oxygen vacancy within the two adjacent tetrahedral sites of fluorite structure surrounding the oxygen migration path. Vacancy formation energies, dopant–vacancy association energies, and migration energies were calculated to elucidate the doping effects on oxygen ion conduction. The migration energies show remarkable dependences on the ionic radii of the cations located at the edges of the migration path. A simple relation between migration energy and vacancy formation energy is proposed. This work provides an informative insight into vacancy diffusion that could be useful in optimizing doping materials for improving oxygen ion conductivity in doped ceria.

(Some figures may appear in colour only in the online journal)

## 1. Introduction

Fluorite structure is a face-centered-cubic arrangement of cations with anions occupying all the tetrahedral holes. This structure is rather open as it introduces large vacant octahedral holes. These voids will be significant when we consider ionic diffusion through the defect structure [1]. Therefore, materials that possess a cubic fluorite structure are known as good candidates for solid electrolytes. Yttria-stabilized zirconia (YSZ) is one of the widely used solid electrolyte materials, as it has high ionic conductivity at high temperature. However, as the operating temperature is reduced the ionic conductivity also decreases significantly. Pure ceria ($CeO_2$) also has the fluorite structure. Oxygen ion conduction takes place by migration via oxygen ion vacancies [2]. The lack of availability of oxygen vacancy formation, which determines the density of mobile oxygen ions, is one of the reasons behind the poor ionic conductivity in pure ceria. Therefore, aliovalent dopants, with lower oxidation number than cerium, are used to enhance oxygen vacancy formation to compensate excess charges and maintain neutrality of the system. Significant improvement can be achieved by introducing rare-earth trivalent cations as the dopants. Experimentally, below 600 °C, the oxygen ion conductivity of doped ceria was found to be two to three orders of magnitude higher than that of YSZ [3].

There are a number of studies on ionic conductivity in doped ceria [2–21]. Kim [6] studied the relationship between the lattice parameter and ionic conductivity of doped ceria. It was found that reducing the lattice deviation leads

 

to a reduction of the internal strain of doped ceria, and therefore increases the ionic conductivity. Gerhard-Anderson *et al* suggested that dopant–vacancy association energy is strongly related to the ionic radius of the dopant [4]. It was found that doping ions with small radii among the lanthanoid series led to strong association and hence the dopants would trap the oxygen vacancies at their nearest neighbor (NN), $D_{vac}^{NN}$, or next nearest neighbor (NNN), $D_{vac}^{NNN}$, sites. Butler *et al* [5] confirmed a qualitative dependency of the association energy on the dopant ionic radius through computations using a Born-like empirical potential model. Recent calculations with empirical potential models were also reported by Wei *et al* [16] to confirm that dopants with small ionic radii have a tendency to attract oxygen vacancies while strong association between an oxygen vacancy and $Ce^{4+}$ was observed for dopants with larger ionic radii where the crossover is exactly at $Gd^{3+}$. Among the lanthanoid series, Yahiro *et al* [7] experimentally confirmed that Sm and Gd-doped ceria (known as SDC and GDC, respectively) showed the highest electrical conductivity because of the close ionic radii of $Sm^{3+}$ (121.9 pm) and $Gd^{3+}$ (119.3 pm) to the radius of $Ce^{4+}$ (111 pm). These results showed that doping ceria with larger or smaller ions than $Sm^{3+}$ and/or $Gd^{3+}$ in the lanthanoid series caused a decrease in ionic conductivity due to the trapping effects of the oxygen vacancies by the dopant ions as indicated by the dopant–vacancy association energies.

For further understanding at atomic level, based on quantum mechanics, density functional theory (DFT) approach is used. A DFT study on the migration energies of Y-, La-, and Sm-doped ceria was reported by Yoshida *et al* [11]. Andersson *et al* reported the relation of the association energy and the migration barrier with the atomic number, and hence ionic radius, of various dopants in the lanthanoid series for particular dopant–vacancy configurations in ceria [22]. It was shown that SDC and GDC can be considered as the best candidates for the dopant, which is also in agreement with the experiment by Yahiro *et al* [7]. Further DFT studies were also reported by Nakayama *et al*, where they have calculated the effect of local atomic arrangements on the defect association and migration energy as Sc, Y, La, Nd, Sm, Gd, Dy, and Lu were chosen for the cation dopants [15]. Some DFT + $U$ studies also reported the migration barriers for every possible migration path of Pr-, Gd-, and Sm-doped ceria respectively [17–19].

Brief discussions on co-doped ceria by means of DFT analysis were also reported in [11, 22] as well as by some experimental studies [3, 8, 10, 12, 13, 20, 23–26]. It was found that co-doping could enhance the oxygen ionic conductivity of ceria-based electrolytes. Yamamura *et al* [10] suggested that local ordering of the oxygen vacancies affects the total oxygen ion conductivity in terms of configurational entropy of multi-doped systems. It was concluded, in general, that co-doping might suppress the ordering of oxygen vacancies, and therefore improve the ionic conductivity. So far, experimentally, co-doped ceria with Sm–Gd (SGDC) and Gd–Y (YGDC) have been found to present higher conductivities than any singly doped ceria [3, 8, 23–25]. Although there is a recent work of atomistic calculations with adjustable empirical parameters by assuming Born-like potentials for Sm–Y, Sm–Gd, and Y–Gd-doped ceria [27], first-principles based study beyond the assumptions has never been reported for co-doped ceria.

In this work we performed first-principles DFT calculations on SGDC to analyze co-doping effects on geometric reconstruction, vacancy formation energy, defect association energy, and oxygen vacancy migration energy. Although the current DFT calculations were performed for the electronic ground state, it is assumed that thermal electronic excitations do not significantly change the charge distribution from the ground state and hence the temperature dependence of the potential energies is negligible. The defect association energy is discussed in terms of the dopant–vacancy interactions. We show that the vacancy formation energies and the migration energies have a strong relationship to the defect association energies, which also depend on the ionic radii of the dopants. The dependency of migration energies on the ionic radii of the cations at the edges of the migration path is also discussed. In the appendix, we show that the $+U$ corrections to the DFT on the energetic trends result in an accordant energy shift.

## 2. Computational methods

All calculations were performed based on spin-polarized DFT using a plane wave basis set as implemented in the Vienna *ab initio* simulation package (VASP) [28, 29]. The projector augmented wave (PAW) method [30] was used, and the exchange–correlation effects were described by the generalized gradient approximation (GGA) using the Perdew–Burke–Ernzerhof (PBE) functional [31]. We initially confirmed that the total energy for pure ceria ($CeO_2$) was converged within 0.1 meV at 520 eV of cut-off energy and $3 \times 3 \times 3$ $k$-points of Monkhorst–Pack [32] meshes centered at the $\Gamma$ point, and then applied these parameters to the further calculations. For charged systems, the total number of electrons is controlled by introducing a homogeneous background charge so as to maintain the charge neutrality of the system.

The supercell was constructed by repetition of the unit cell of ceria with space group $Fm\bar{3}m$. Thus the supercell consists of 32 Ce and 64 O atoms for pure ceria. Full optimization of the atomic positions and lattice parameters was performed by minimizing the Hellman–Feynman forces acting on each ion to be less than 0.02 eV $Å^{-1}$ [33], and a Gaussian smearing of 0.2 eV was employed for calculating partial occupancies. Note that in previous works [15, 18, 22] the volume of the supercell was kept constant and equal to the calculated volume of the pure ceria assuming that structural relaxation only affects the local surrounding of the defects. However, in this work we consider full geometry relaxations as in the experiments changes in the lattice parameters were observed due to the doping [6, 12, 13, 21]. To obtain accurate total energies, then, after geometry relaxations, static calculations were performed by the tetrahedron method with Blöchl correction [34]. Point defects were modeled by substitutions of two Ce atoms with either Sm or Gd atoms and removal of one vacancy atom was made per supercell, namely,

$Ce_{0.94}Sm_{0.06-x}Gd_xO_{1.97}$, for $x = 0$ (SDC), 0.03 (SGDC), and 0.06 (GDC).

The migration energies for an oxygen ion in the defect structures were determined by the total energy difference between a configuration for the initial position of the migrating oxygen and that for the saddle point of the corresponding migration path. The migration paths were observed to follow a straight line. The optimal saddle point positions were obtained by giving the initial position of the migrating oxygen halfway between the oxygen sites of the migration process and then relaxing within the perpendicular plane to the path while the lattice parameters were fixed [17–19, 22]. The reliability of this method was confirmed by calculations for positions slightly shifted from halfway along the path. The approximated errors in determining these migration energies are less than ∼10 meV.

To confirm the effects of $+U$ corrections to DFT, the standard GGA + $U$ method for the Coulomb repulsion and exchange interaction formulated by Dudarev *et al* [35] to consider the localization effects of Ce 4f electrons was used. The conventional DFT is sufficient for discussions in the present work despite the changes in energies; conventional DFT shows a systematic dependence on the ionic radii and produces the same trend as DFT + $U$ (details are explained in the appendix).

## 3. Results and discussion

### *3.1. Crystal structures*

Pure bulk ceria possesses the fluorite structure where the cations ($Ce^{4+}$) reside at the face-centered-cubic (fcc) arrangement and the anions ($O^{2-}$) occupy the tetrahedral holes, each of which is coordinated with four cations as shown in figure 1(a). Here we consider three initial configurations distinguished by the dopant–dopant distances, $D_1D'_1(1) = D^{NN}_{vac}$–$D'^{NN}_{vac}$ (1), $D_1D'_2(2) = D^{NN}_{vac}$ –$D'^{NNN}_{vac}$ (2), and $D_1D'_2(3) = D^{NN}_{vac}$–$D'^{NNN}_{vac}$(3) as shown in figures 1(b)–(d), respectively, where the bracketed digit indicates the distance between two dopants either at first NN, second NN, or third NN, and the right-hand-side of each equation denotes a synonym by abbreviation as $D_1 = D^{NN}_{vac}$ and $D_2 = D^{NNN}_{vac}$. The prime superscript is used to distinguish between the dopant species. For example, in SGDC, D is assigned to Gd and D′ to Sm. There are eight paths for migration between NN sites of dopant atoms as depicted in figures 1(e)–(l):

$$\text{(i) } D_1D'_1(1) \rightarrow D'_1D_1(1) = DD'(11)$$
$$\text{(ii) } D_1D'_1(1) \rightarrow D_2D'_2(1) = DD'(12)$$
$$\text{(iii) } D_1D'_1(1) \rightarrow D_1D'_2(1) = DD'(13)$$
$$\text{(iv) } D_1D'_1(1) \rightarrow D_2D'_1(1) = DD'(14)$$
$$\text{(v) } D_1D'_2(2) \rightarrow D_2D'_1(2) = DD'(21)$$
$$\text{(vi) } D_2D'_1(2) \rightarrow D_1D'_2(2) = DD'(22)$$
$$\text{(vii) } D_1D'_2(3) \rightarrow D_2D'_1(3) = DD'(31)$$
$$\text{(viii) } D_2D'_1(3) \rightarrow D_1D'_2(3) = DD'(32).$$

The changing order of D symbols makes equivalent configurations in the mirror image and path (i) is a transition between mirror images, as their distinction may be made by describing the final one as $D'_1D_1$. Note that in DD′(14), DD′(22), and DD′(32) the positions of Gd and Sm dopants with respect to the vacancy are interchanged (see figures 1(g)–(l)), i.e., DD′(14) ≡ D′D(13), DD′(22) ≡ D′D(21), and DD′(32) ≡ D′D(31). In the case of DD′(13) and DD′(14), for SGDC, we have GS(13) and GS(14), where $G_1S_1(1) \rightarrow G_1S_2(1) = GS(13)$ and $G_1S_1(1) \rightarrow G_2S_1(1) = GS(14)$. If we interchange Gd and Sm positions in GS(14) then it becomes $S_1G_1(1) \rightarrow S_2G_1(1) = SG(14) = GS(13)$.

**Table 1.** Lattice constants of pure and doped ceria.

| Material | DFT calculations for $D^{NN}_{vac}$–$D'^{NN}_{vac}$ (NN) (Å) | Experiment (Å) [12, 13] |
|---|---|---|
| Pure ceria | 5.463 | 5.412 |
| SDC | 5.469 | 5.432[a] |
| GDC | 5.465 | 5.423[b] |
| SGDC | 5.466 | 5.426[c], 5.429[d] |

[a] $Ce_{0.85}Sm_{0.15}O_{1.925}$.
[b] $Ce_{0.85}Gd_{0.15}O_{1.925}$.
[c] $Ce_{0.85}Sm_{0.05}Gd_{0.10}O_{1.925}$.
[d] $Ce_{0.85}Sm_{0.10}Gd_{0.05}O_{1.925}$.

We first performed atomic relaxations and obtained optimized lattice parameters as shown in table 1. The optimized lattice constants are shown for SDC, GDC, and SGDC with a vacancy per supercell, where the lattice deviation decreases in the order of SDC > SGDC > GDC > pure ceria. The deviation is due to the ionic radius mismatch of each dopant with the host cation, which decreases in the order of $Sm^{3+}$ > $Gd^{3+}$. Experimentally, it was reported that the lattice constants vary almost linearly with the dopant concentrations [12, 13]. We deduced the corresponding experimental values for the calculated concentrations and obtained 5.416 Å, 5.420 Å for GDC and SDC, respectively. Thus the estimated deviations are ∼0.004 and ∼0.008 Å for GDC and SDC with respect to pure ceria. The optimized structures in the present work give 0.002 Å and 0.006 Å deviations for GDC and SDC, respectively, while that for SGDC lies between GDC and SDC lattice constants. These deviations originated from the local atomic rearrangements around the vacancy as shown in figures 1(b)–(d). Remarkable displacements were observed on NN oxygen atoms approaching the vacancy site. The six oxygen atoms at NN sites of the vacancy shifted toward the vacancy by 0.08–0.23 Å, 0.17–0.26 Å, and 0.16–0.27 Å in $D_1D'_1(1)$, $D_1D'_2(2)$, and $D_1D'_2(3)$, respectively.

### *3.2. Defect association and vacancy formation energy*

In this section we discuss two important factors that will determine the oxygen ion conductivity in doped ceria: (i) the dopant–vacancy association energy $E_{ass}$; and (ii) the oxygen vacancy formation energy $E^f_{vac}$. Both contribute to the availability of the free oxygen vacancies, which will determine the availability of mobile oxygen ions for ionic conductivity. The dopant–vacancy association is defined as an interaction between the oxygen ion vacancies and aliovalent

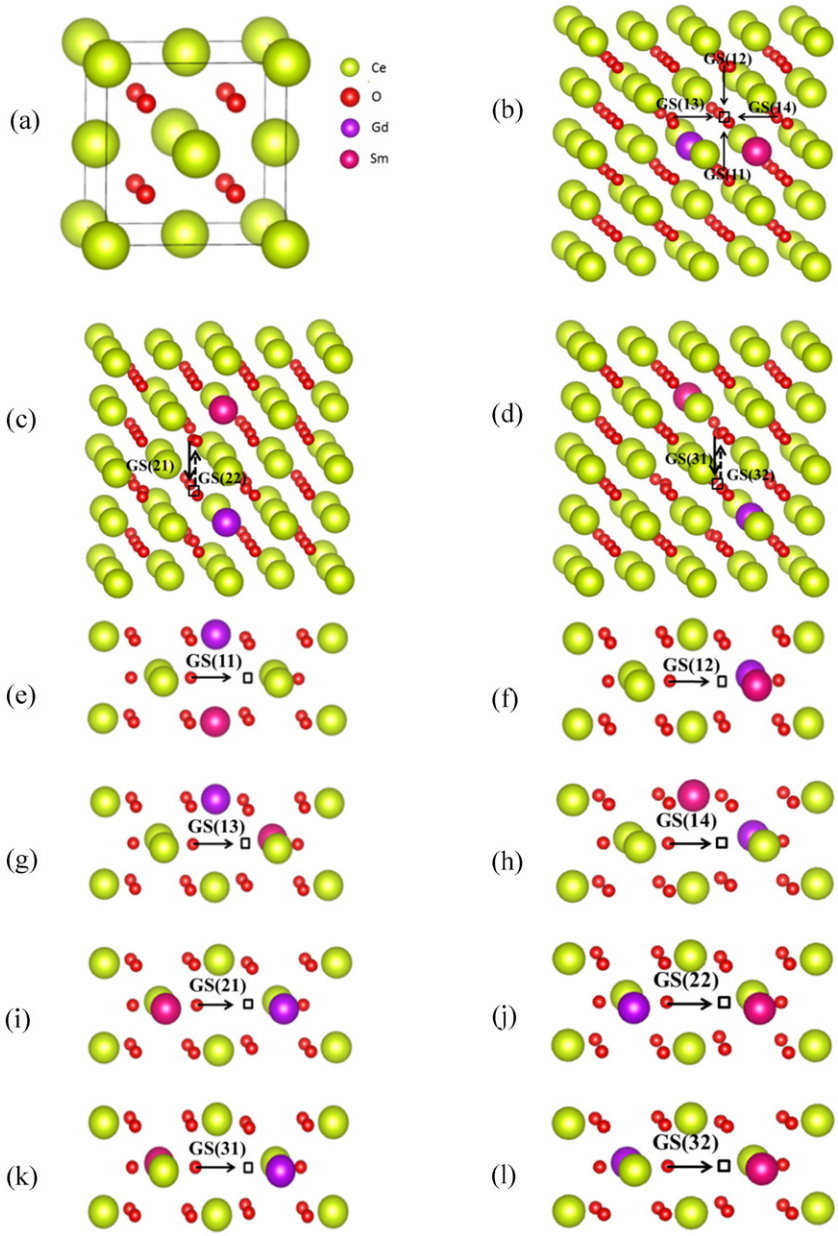


**Figure 1.** Geometry structure of pure ceria (a), three SGDC configurations (b)–(d), and the first coordination shells enclosing the migration paths (e)–(l). Arrows indicate directions of oxygen migration toward the vacancy indicated by a square box (the dashed arrows indicate the reverse migrations). Configuration $G_1S_1(1)$ is shown in (b) with migration paths (e) GS(11), (f) GS(12), (g) GS(13), and (h) GS(14). Configuration $G_1S_2(2)$ is shown in (c) with migration paths (i) GS(21) and (j) GS(22). Configuration $G_1S_2(3)$ is shown in (e) with migration paths (k) GS(31) and (l) GS(32).

cations. The interaction is mainly due to Coulomb attraction between the dopants and vacancies due to their effective charges in the lattice. Often such interactions are evaluated by assuming that the constituent defects are isolated from one another; this is known as the dilute limit. $E_{ass}$ in $D_{vac}^{NN}$ and $D_{vac}^{NNN}$ is defined by

$$E_{ass} = E_{D+vac} + E_{CeO_2} - E_{vac} - E_D \quad (1)$$

where D is the dopant (D = Sm, Gd), $E_{D+vac}$ is the total energy of the supercell containing the dopant–vacancy complex, $E_D$ and $E_{vac}$ are the total energies of the supercells with isolated dopant and vacancy, respectively, and $E_{CeO_2}$ is the total energy per formula unit of the 96 atom supercell of ideal cubic fluorite. A positive value of $E_{ass}$ indicates repulsive interaction between dopant and vacancy (negative value corresponds to a binding energy). $E_{vac}^{f}$ is defined as the energy needed to remove an oxygen atom in the form of half an oxygen molecule from ceria and is formulated as

$$E_{vac}^{f} = E_{D+vac} - E_D + 1/2E_{O_2} \quad (2)$$

where $E_{O_2}$ is the chemical potential of $O_2$.

In this study we consider configurations that are chosen to focus on the cation effect on the first coordination shell enclosing the migration path shown in figures 1(e)–(l). First,

**Table 2.** Defect association energies for SDC and GDC calculated from equation (1).

| Structure | $E_{ass}$ (eV) | Configuration |
|---|---|---|
| SDC | 0.204 (0.080)[a] | $D^{NN}_{vac}$ |
| | 0.236 | $D^{NNN}_{vac}$ |
| GDC | 0.142 (0.040)[a] | $D^{NN}_{vac}$ |
| | 0.249 | $D^{NNN}_{vac}$ |

[a] Values obtained from fixed volume calculations as pure ceria.

we calculate the defect association energies for a single dopant ion at the NN and NNN sites from the vacancy (see table 2). It is found that the NN site is more favorable for Sm by ∼0.03 eV and for Gd by ∼0.11 eV than the NNN site. It is also found that the NN site of Gd is more favorable than Sm by ∼0.06 eV. We therefore see in table 3 for co-doped ceria that $G_1S_2(2)$ and $G_1S_2(3)$, in terms of relative total energies, $\Delta E_{DFT}$, are more stable than $G_2S_1(2)$ and $G_2S_1(3)$ by ∼0.08 eV, where $\Delta E_{DFT}$ is defined as the energy difference relative to the lowest total energies.

The calculated values of the vacancy formation energies are shown for each configuration in table 3. Note that the negative value of the vacancy formation energy indicates the instantaneous formation of the oxygen vacancy when two trivalent cations substituted $Ce^{4+}$ ion sites to maintain charge neutrality of the system. The lowest $E^f_{vac}$ for the neutral vacancy is found in $G_1G_1(1)$ followed by most of SGDC and then SDC. $G_1G_2(2)/G_1G_2(3)$ have higher $E^f_{vac}$ than $G_1G_1(1)$ due to higher $G^{NNN}_{vac}$ association compared with $G^{NN}_{vac}$ association by ∼0.1 eV. However, the quantitative coincidence with $S_1S_1(1)$ may be accidental. We also found that the vacancy formation is easier in $G_1S_2(2)/G_1S_2(3)$, where the vacancy is at the NN site of Gd, rather than $G_2S_1(2)/G_2S_1(3)$, where the vacancy is at the NN site of Sm, as indicated by $D^{NN}_{vac}$ association. Therefore, higher dopant–vacancy association tends to increase the vacancy formation energy. Low vacancy formation energy indicates the ease of vacancy formation, leading to an enhancement of the availability of mobile oxygen ions.

Another observation we found for preliminary comparison is (in table 2) that $D^{NN}_{vac}$ association decreases by ∼0.12 eV for SDC and ∼0.10 eV for GDC as we assumed the cell volume fixed to be the same as for pure ceria. Also, the calculated $E^f_{vac}$ for $S_1S_1(1)$ and $G_1G_1(1)$ for fixed volume are −0.571 eV and −0.667 eV, respectively (increases by ∼0.32 eV compared to the unstrained one, as can be seen in table 3). As in the experiment where there was no strain put to the lattice, which led to lattice deformation [12, 13], our calculation results suggest that fixing the volume to the same as pure ceria would enforce a lattice strain on the actual system which may lead to a change in the dopant–vacancy interactions and the ease of the vacancy formations.

### *3.3. The vacancy migration energy*

The calculated migration energies for each migration path are shown in table 4. The lowest migration barrier is found in GS(22) and GS(32) followed by GS(21) and GS(31) and GS(12). In these configurations, Ce–Ce pair cations are located across the migration path (see figure 1). As we introduce dopants into these pair cations, i.e. Gd–Ce, Sm–Ce, or Sm–Gd, the migration barrier increases. Referring back to the association energies (see table 3), it is understood that the low migration energies of GS(22) and GS(32) are due to strong repellency of Sm cations against oxygen vacancies compared to Gd cations as in GS(21)and GS(31). Notice that the differences of the migration energies between GS(21) and GS(31), and GS(22) and GS(32), are negligibly small. This indicates that the dopant–vacancy association dominate the interaction in determining the migration energy rather than the dopant–dopant interaction. However, careful discussion must be addressed to GS(11), GS(13), and GS(14) which share the same association energy with GS(12) while having higher migration energies.

**Table 3.** Relative energies (whose origin is the lowest one among the same compositions), vacancy formation energies, and defect association energies of doped ceria.

| Structure | $\Delta E_{DFT}$/eV per cell | $E^f_{vac}$ (eV) | $E_{ass}$ (eV) | Cation–cation distance[a] (Å) | Configuration[b] |
|---|---|---|---|---|---|
| $S_1S_1(1)$ | 0.015 | −0.892 | 0.457 | 3.864 | $D^{NN}_{vac}$–$D'^{NN}_{vac}$ |
| $S_1S_2(2)$ | 0.037 | −0.868 | 0.475 | 5.464 | $D^{NN}_{vac}$–$D'^{NNN}_{vac}$ |
| $S_1S_2(3)$ | 0.000 | −0.875 | 0.477 | 6.692 | $D^{NN}_{vac}$–$D'^{NNN}_{vac}$ |
| $G_1G_1(1)$ | 0.000 | −0.987 | 0.309 | 3.864 | $D^{NN}_{vac}$–$D'^{NN}_{vac}$ |
| $G_1G_2(2)$ | 0.081 | −0.892 | 0.407 | 5.464 | $D^{NN}_{vac}$–$D'^{NNN}_{vac}$ |
| $G_1G_2(3)$ | 0.066 | −0.893 | 0.411 | 6.692 | $D^{NN}_{vac}$–$D'^{NNN}_{vac}$ |
| $G_1S_1(1)$ | 0.013 | −0.940 | 0.381 | 3.864 | $D^{NN}_{vac}$–$D'^{NN}_{vac}$ |
| $G_1S_2(2)$ | 0.022 | −0.918 | 0.405 | 5.464 | $D^{NN}_{vac}$–$D'^{NNN}_{vac}$ |
| $G_2S_1(2)$ | 0.097 | −0.843 | 0.479 | 5.464 | $D^{NN}_{vac}$–$D'^{NNN}_{vac}$ |
| $G_1S_2(3)$ | 0.000 | −0.920 | 0.407 | 6.692 | $D^{NN}_{vac}$–$D'^{NNN}_{vac}$ |
| $G_2S_1(3)$ | 0.073 | −0.848 | 0.479 | 6.692 | $D^{NN}_{vac}$–$D'^{NNN}_{vac}$ |

[a] The distance was taken from the ideal lattice before geometry relaxation.

[b] The NN distance is ∼2.4 and the NNN ∼4.5 Å.

**Table 4.** Migration energies of doped ceria. Forward migrations indicate an oxygen vacancy jump from left to right in figure 1 and its reverse direction. DD′(22) and DD′(32) are in the reverse direction of DD′(21) and DD′(31), respectively.

| | Migration energy (eV) | |
|---|---|---|
| Migration path | Forward | Backward |
| SS(12) | 0.415 | 0.374 |
| SS(21) | 0.386 | 0.386 |
| SS(31) | 0.389 | 0.389 |
| GG(12) | 0.510 | 0.313 |
| GG(21) | 0.410 | 0.410 |
| GG(31) | 0.409 | 0.409 |
| GS(11) | 0.976 | 0.976 |
| GS(12) | 0.456 | 0.336 |
| GS(13) | 0.517 | 0.492 |
| GS(14) | 0.628 | 0.525 |
| GS(21) | 0.436 | 0.362 |
| GS(31) | 0.435 | 0.362 |

The difference of the migration energies between GS(11) and GS(14) can be explained in terms of the ionic radii of cations at the edges of the migration path [2, 4–6, 22, 36]. As the ionic radii are larger than that of the host cation, the room available for migration is reduced. It is found that, when the Ce–Ce pair is situated at the edges of the migration path, the migration barrier is smaller compared to the ones where the Gd–Ce, Sm–Ce, and Sm–Gd pairs reside at the edges. This tendency is clearly observed in the results for both the forward and backward directions of oxygen ion migration for each configuration. It is also shown by the geometry relaxations at the saddle point that displacements of the edge cations vary with the ionic radii of the cations. Largest displacements at the saddle point, with respect to its initial position, are experienced by Sm and Gd atoms in GS(11), by ∼0.135 Å, followed by Sm and Ce atoms in GS(14), by ∼0.120 and ∼0.115 Å, Gd and Ce atoms in GS(3), by ∼0.119 and ∼0.105 Å, and Ce atoms in GS(12), by ∼0.100 Å. Hence, the energy needed to relax the cations at the edges enhances the migration energies and decreases in the order of (Sm–Gd) > (Sm–Ce) > (Gd–Ce) > (Ce–Ce). This indicates that ionic radii play a crucial role in the atomic relaxations of the edge cations in determining the migration energies.

The migration energies of SDC and GDC were also calculated and compared to the co-doped one (see from SS(12) to GG(31) in table 4). The results show that the migration energy of GS(12) lies between SS(12) and GG(12). This again can be explained by the dopant–vacancy interaction in NN configurations. SS(12) has the lowest forward migration energy, followed by GS(12) and GG(12), respectively, while GG(12) has the lowest backward migration energy. For the same feature as SGDC in GS(21)/GS(31), for SS(21)/SS(31) in SDC, and GG(21)/GG(31) in GDC, the dopant–dopant distance results in similar migration energies. It is also found that GS(21) and GS(31) migration energies are higher than both SDC and GDC while GS(22) and GS(32) migration energies are the lowest. We might initially expect that GS(21)/GS(31) and GS(22)/GS(32) migration energies lie between SS(21)/SS(31) and GG(21)/GG(31). However, due to the competing association interactions between $D_{vac}^{NN}$ and $D_{vac}^{NNN}$, the dopant–vacancy association cannot be described as a simple superposition of each constituent. The obtained dopant–vacancy association involves both NN and NNN interaction at the same time and the two-dopant $E_{ass}$ describes the local interaction in the first coordination shell enclosing the migration path.

From the trend in migration energies $E_m$ there seems to be a simple relation that can be drawn between $E_m$ and $E_{vac}^{f}$. For convenience in designing new ceria-based materials, we propose a simple relation of the migration energy for the oxygen ion jump within two adjacent tetrahedral sites between doped ceria for the same dopant configuration and different compositions; in our case this is for Sm and Gd dopants,

$$E_m(x) = E_m(x_0) + \{E_{vac}^{f}(x_0) - E_{vac}^{f}(x)\} \quad (3)$$

$E_m(x)$ is the predicted migration energy and $E_{vac}^{f}(x)$ is the vacancy formation energy corresponding to the $x$ configuration while $x_0$ is assigned as the reference compositions of doped ceria. This expression says that the migration energy in doped ceria is fundamentally determined by the formation energy because the migration paths should be chosen to be across Ce–Ce pairs whose barrier is the lowest and independent of doping. This expression does not hold for cases where $x_0$ denotes undoped (reduced) ceria. Here we simulate a procedure where we first have data of migration and formation energies in SDC, next obtain the formation energies of new materials, and then predict migration energies of the new materials by equation (3). For instance, the predicted migration energies of GG(12) and GS(12) (SS(12) as the reference) are 0.510 eV and 0.463 eV, respectively. The predicted migration energies of GG(21) and GS(22) (SS(21) as the reference) are 0.410 eV and 0.361 eV, respectively. These predictions show good accordance with the DFT calculation results within an error of ∼10 meV. Although the above relation has been confirmed only among SDC, GDC, and SGDC, and further refinement of the background theory is desired, equation (3) is expected to be applicable to various ceria-based materials. Thus, enabling the prediction of the migration energy would be beneficial for further designing materials of oxygen ion conductors.

## 4. Summary

Defect association and oxygen migration in SGDC have been studied by means of first-principles DFT calculations. From the discussion of $E_{vac}^{f}$ and $E_{ass}$, the most favorable site for oxygen vacancy formation was found to be at the NN site of Gd in SGDC when Gd and Sm are not NN to one another. The calculated migration energies show dependency on both $E_{ass}$ and ionic radii of the edge cations. Higher $E_{ass}$ gives lower migration energy. Larger ionic radii of the edge cations result in higher migration energy due to the energy needed to relax the edge cations to create room for migration. However, due to the competing association interactions between $D_{vac}^{NN}$ and $D_{vac}^{NNN}$, which is beyond the simple logic of superposition, correlations of the dopant–vacancy association energies with the vacancy formation energies and the migration energies

are weak in comparison among SGDC, SDC, and GDC. This means that the dopant–vacancy association involves both NN and NNN interactions at the same time and the two-dopant $E_{ass}$ describes the local interactions in the first coordination shell enclosing the migration path. It is noted that the dopant–vacancy association dominates the interactions in determining the migration energy rather than the dopant–dopant interaction. Finally, we noticed a linear relationship between $E^{f}_{vac}$ and $E_m$ that could give an insight to predict and optimize co-doping species in designing ceria-based solid electrolytes.

## Acknowledgments

This work is supported by JST (Japan Science and Technology Agency) through ALCA (Advanced Low Carbon Technology Research and Development) Program 'Development of novel metal–air secondary battery based on fast oxide ion conductor nano thickness film' and Elements Science and Technology Project 'New development of self-forming nano-particle catalyst without precious metals'. Some of the calculations presented here were done using the computer facilities at ISSP Supercomputer Center (University of Tokyo). MA would like to thank the DGHE (Directorate General of Higher Education) of Indonesia for the financial study aid granted to him. Discussions with M Nakayama from the Department of Materials Science and Engineering, Nagoya Institute of Technology, and D Andersson from the Materials Science and Technology Division, Los Alamos National Laboratory, are gratefully acknowledged.

## Appendix

Table A.1 shows the calculated $E^{f}_{vac}$ and migration energies for selected configurations. Here we only consider the $D_1D_1(1)$ type of system. DFT + $U$ calculations resulted in different absolute values of energies, however, the same trend in differences between different compositions as for conventional DFT were reproduced. $G_1G_1(1)$ has the lowest $E^{f}_{vac}$ of the neutral vacancies while $G_1S_1(1)$ and $S_1S_1(1)$ come second and third. Also for the migration energies, GS(12) lies in between SS(12) and GG(12), where SS(12) is the lowest. Consequently, the $+U$ correction resulted in only comparable energy shift ∼31–40 meV for $E^{f}_{vac}$, ∼ 70–75 meV for forward migrations, and 16–26 meV for backward migrations. It is noticed that equation (3) is still valid for DFT + $U$ calculation results where the predicted migration energies differ by less than ∼12 meV.

## References

[1] Trovarelli A 2002 *Catalysis by Ceria and Related Materials* (London: Imperial College Press)
[2] Inaba H and Tagawa H 1996 Ceria-based solid electrolytes *Solid State Ion.* **83** 1–16
[3] Mogensen M, Sammes N M and Tompsett G A 2000 Physical, chemical and electrochemical properties of pure and doped ceria *Solid State Ion.* **129** 63–94
[4] Gerhardt-Anderson R and Nowick A S 1981 Ionic conductivity of $CeO_2$ with trivalent dopants of different ionic radii *Solid State Ion.* **5** 547–50
[5] Butler V, Catlow C R A, Fender B E F and Harding J H 1983 Dopant ion radius and ionic conductivity in cerium dioxide *Solid State Ion.* **8** 109–13
[6] Kim D-J 1989 Lattice parameters, ionic conductivities, and solubility limits in fluorite-structure $MO_2$ oxide [M = $Hf^{4+}$, $Zr^{4+}$, $Ce^{4+}$, $Th^{4+}$, $U^{4+}$] solid solutions *J. Am. Ceram. Soc.* **72** 1415–21
[7] Yahiro H, Eguchi K and Arai H 1989 Electrical properties and reducibilities of ceria-rare earth oxide systems and their application to solid oxide fuel cell *Solid State Ion.* **36** 71–5
[8] Mori T, Ikegami T and Yamamura H 1999 Application of a crystallographic index for improvement of the electrolytic properties of the $CeO_2$–$Sm_2O_3$ system *J. Electrochem. Soc.* **146** 4380–5
[9] Kilner J A 2000 Fast oxygen transport in acceptor doped oxides *Solid State Ion.* **129** 13–23
[10] Yamamura H, Katoh E, Ichikawa M, Kakinuma K, Mori T and Haneda H 2000 Multiple doping effect on the electrical conductivity in the $(Ce_{1-x-y}La_xM_y)O_{2-\delta}$ (M = Ca, Sr) system *Electrochem.* **68** 455–9
[11] Yoshida H, Inagaki T, Miura K, Inaba M and Ogumi Z 2003 Density functional theory calculation on the effect of local structure of doped ceria on ionic conductivity *Solid State Ion.* **160** 109–16
[12] Wang F-Y, Chen S and Cheng S 2004 $Gd^{3+}$ and $Sm^{3+}$ co-doped ceria based electrolytes for intermediate temperature solid oxide fuel cells *Electrochem. Commun.* **6** 743–6
[13] Wang F-Y, Wan B-Z and Cheng S 2005 Study on $Gd^{3+}$ and $Sm^{3+}$ co-doped ceria-based electrolytes *J. Solid State Electrochem.* **9** 168–73
[14] Omar S, Wachsman E D and Nino J C 2008 Higher conductivity $Sm^{3+}$ and $Nd^{3+}$ co-doped ceria-based electrolyte materials *Solid State Ion.* **178** 1890–7
[15] Nakayama M and Martin M 2009 First-principles study on defect chemistry and migration of oxide ions in ceria doped with rare-earth cations *Phys. Chem. Chem. Phys.* **11** 3241–9
[16] Wei X, Pan W, Cheng L and Li B 2009 Atomistic calculation of association energy in doped ceria *Solid State Ion.* **180** 13–7
[17] Dholabhai P P, Adams J B, Crozier P and Sharma R 2010 Oxygen vacancy migration in ceria and Pr-doped ceria: a DFT + $U$ study *J. Chem. Phys.* **132** 094104
[18] Dholabhai P P, Adams J B, Crozier P and Sharma R 2010 A density functional study of defect migration in gadolinium doped ceria *Phys. Chem. Chem. Phys.* **12** 7904–10

**Table A.1.** The vacancy formation energies and migration energies calculated by DFT + $U$.

| | | Migration energy (eV) | |
|---|---|---|---|
| Structure/migration path | $E^{f}_{vac}$ (eV) | Forward | Backward |
| $S_1S_1(1)$/SS(12) | −0.861 | 0.488 | 0.348 |
| $G_1G_1(1)$/GG(12) | −0.947 | 0.580 | 0.287 |
| $G_1S_1(1)$/GS(12) | −0.908 | 0.531 | 0.315 |

[19] Ismail A, Hooper J, Giorgi J B and Woo T K 2011 A DFT + $U$ study of defect association and oxygen migration in samarium-doped ceria *Phys. Chem. Chem. Phys.* **13** 6116–24
[20] Singh N, Singh P, Kumar D and Parkash O 2012 Electrical conductivity of undoped, singly doped, and co-doped ceria *Ionics* **18** 127–34
[21] Omar S, Wachsman E D and Nino J C 2006 A co-doping approach towards enhanced ionic conductivity in fluorite-based electrolytes *Solid State Ion.* **177** 3199–203
[22] Andersson D A, Simak S I, Skorodumova N V, Abrikosov I A and Johansson B 2006 Optimization of ionic conductivity in doped ceria *Proc. Natl. Acad. Sci. USA* **103** 3518–21
[23] Dronskowski R and Bloechl P E 1993 Crystal orbital Hamilton populations (COHP): energy-resolved visualization of chemical bonding in solids based on density-functional calculations *J. Phys. Chem.* **97** 8617–24
[24] Lu Z, Yang Z, He B, Castleton C and Hermansson K 2011 Cu-doped ceria: oxygen vacancy formation made easy *Chem. Phys. Lett.* **510** 60–6
[25] Martin M 2006 On the ionic conductivity of strongly acceptor doped, fluorite-type oxygen ion conductors *J. Electroceram.* **17** 765–73
[26] Hellman O, Skorodumova N V and Simak S I 2012 Charge redistribution mechanisms of ceria reduction *Phys. Rev. Lett.* **108** 135504
[27] Ou D R, Ye F and Mori T 2011 Defect clustering and local ordering in rare earth co-doped ceria *Phys. Chem. Chem. Phys.* **13** 9554–60
[28] Kresse G and Furthmüller J 1996 Efficiency of *ab initio* total energy calculations for metals and semiconductors using a plane-wave basis set *Comput. Mater. Sci.* **6** 15–50
[29] Kresse G and Furthmüller J 1996 Efficient iterative schemes for *ab initio* total-energy calculations using a plane-wave basis set *Phys. Rev.* B **54** 11169–86
[30] Blöchl P E 1994 Projector augmented-wave method *Phys. Rev.* B **50** 17953–79
[31] Perdew J P, Burke K and Ernzerhof M 1996 Generalized gradient approximation made simple *Phys. Rev. Lett.* **77** 3865–8
[32] Monkhorst H J and Pack J D 1976 Special points for Brillouin-zone integrations *Phys. Rev.* B **13** 5188–92
[33] Feynman R P 1939 Forces in molecules *Phys. Rev.* **56** 340–3
[34] Blöchl P E, Jepsen O and Andersen O K 1994 Improved tetrahedron method for Brillouin-zone integrations *Phys. Rev.* B **49** 16223–33
[35] Dudarev S L, Botton G A, Savrasov S Y, Humphreys C J and Sutton A P 1998 Electron-energy-loss spectra and the structural stability of nickel oxide: an LSDA + $U$ study *Phys. Rev.* B **57** 1505–9
[36] Chen H-T and Chang J-G 2010 Oxygen vacancy formation and migration in $Ce_{1-x}Zr_xO_2$ catalyst: a DFT + $U$ calculation *J. Chem. Phys.* **132** 214702